A New Development of an Equivalent Circuit Model for Magnetostatic Forward Volume Wave Transducers

KEN'ICHIRO YASHIRO, MEMBER, IEEE, AND SUMIO OHKAWA, SENIOR MEMBER, IEEE

Abstract—**A new three-port equivalent circuit model of microstip transducers for the generation and detection of magnetostatic forward volume waves (MSFVW) is presented explicitly from fundamental physical considerations. In this circuit model, each microstrip of MSFVW transducers is expressed by a three-port circuit incorporating a series reactance, a lossless transformer, and a lossy transmission line. Circuit parameters are determined in closed forms by the use of solutions of pertinent boundary value problems. Hence, by virtue of the powerful and well-established methods of circuit theory, the three-port circuit can be directly applied to multibar microstrip transducers, of which configurations are of parallel bar, multibar π, meander, etc. Furthermore, the effects of parasitics, for example, capacities of bonding pads, are also easily taken into account. Some typical configurations of transducers are analyzed numerically and compared with experimental results.**

I. INTRODUCTION

MAGNETOSTATIC wave (MSW) devices are potentially useful for signal processing at microwave frequencies [1]. Changing the current state of the art from a promising into a practical one would require that the excitation efficiency, or, equivalently, the radiation impedance, be characterized in terms of geometrical and material parameters. In particular, it is convenient to work with equivalent electric circuits in the analysis and synthesis of MSW devices and in designing matching network. Moreover, the equivalent circuit approach enables us to employ the great power of existing techniques of circuit analysis.

MSW's can be easily excited by a microstrip due to the strong coupling between the MSW and a current on the microstrip. By means of the standard Fourier transform, Ganguly and Webb [2] have analyzed the magnetostatic surface waves (MSSW's) excited by a single microstrip to obtain an equivalent radiation resistance. Following the procedure of Ganguly and Webb, the excitation of the other modes, i.e., magnetostatic forward volume wave (MSFVW) [3] and magnetostatic backward volume wave (MSBVW) [4], has also been analyzed. Furthermore, the method has been developed to manifest the radiation characteristics of various transducers by using an array factor for the noninteracting current sources [5]–[11] and to include the effect of the finite width of ferrimagnetic film [12], [13]. However, Emtage [14] showed that MSW's emitted by one part of the transducer react on the other part because of the strong coupling. Owens *et al.* [15] developed a three-port model including the effects of mutual interaction between the transducer strips, and bidirectional propagation of MSFVW's. In their model, each transducer strip was represented by a black box, which was characterized by a scattering matrix, and was connected with others in parallel. The three-port model for the MSFVW transducer herein is represented by an equivalent circuit containing a frequency-dependent series reactance, a frequency-dependent lossless transformer, and a lossy transmission line. Consequently the multibar π and meander transducers as well as the multibar parallel transducer can be easily analyzed taking the coupling between transducer strips into account to some extent. As will be shown, the electric ports connected in series, parallel, or hybrid are ready to be analyzed. Moreover, the model not only makes it possible to estimate the propagation loss automatically since the MSFVW propagation path is modeled as a lossy transmission line, but also includes effects such as parasitic capacitance and the skin effect. We will adopt a current distribution on a transducer strip, which satisfies the edge condition, more realistic than a uniform one.

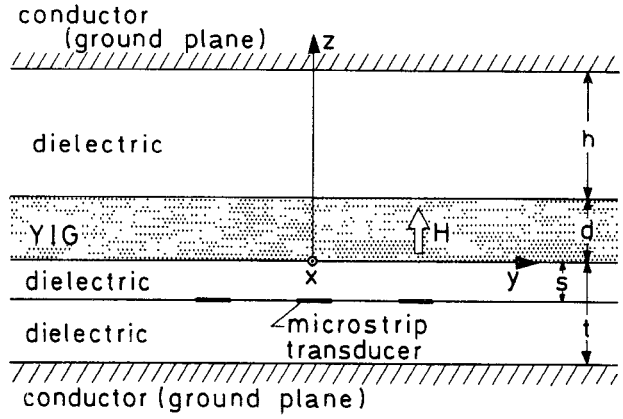

Fig. 1. Model geometry for MSFVW transducer.

In this paper we consider the excitation geometry shown in Fig. 1. The "flipped" and "wire-over" configurations given by Ownes *et al.* [1] can be obtained from this general structure by taking either the upper or the lower ground plane in Fig. 1 to infinity. The derivation of equivalent

Manuscript received August 3, 1987; revised December 8, 1987.
The authors are with the Department of Electronic Engineering, Chiba University, 1-33, Yayoi-cho, Chiba, 260 Japan.
IEEE Log Number 8820434.

0018-9480/88/0600-0952$01.00 ©1988 IEEE

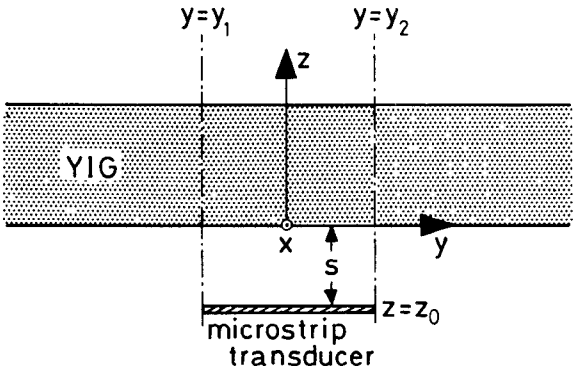

Fig. 2. Microstrip section.

circuits is based on the assumptions that the fields are uniform along the x axis and that microstrip transducers are shorted at one end.

II. Preparation

As a preparation for construction of an equivalent circuit model, we will analyze the MSFVW excited by a single microstrip transducer, mostly in the same manner as Ganguly and Webb did [2]. Suppose that the magnetic field is represented as the gradient of a potential, $\boldsymbol{h}=\nabla\phi$, and that all field quantities have a time variation given by $\exp(j\omega t)$, where ω is the angular frequency. The Fourier transform is applied to ϕ with respect to y (Fig. 1). The normal component of the magnetic flux density vanishes at the metal surface and continuity of the potential and the normal magnetic flux density is required at the YIG–dielectric interface. A discontinuity of tangential magnetic field must be accounted for by a current distribution on the strip (Fig. 2). By imposing the boundary conditions, the potential function is obtained in terms of $I_0 J_x(\beta)$, where I_0 is the total current flowing on the strip and $J_x(\beta)$ is the Fourier transform of a normalized current distribution $j_x(y)$ so that

$$\int_{y_1}^{y_2} j_x(y)\,dy = J_x(0) = 1. \tag{1}$$

The calculus of residues of the integrand at poles yields the desired potential expression. Then for each mode propagating in the positive y direction, ϕ is given by

$$\phi(y,z) = AI_0 g(z) e^{-j\beta y} \tag{2}$$

where

$$g(z) = \begin{cases} \left(\cos\dfrac{\beta d}{a} + a\tanh\beta t\sin\dfrac{\beta d}{a}\right) \cdot \dfrac{\cosh\beta(z-h-d)}{\cosh\beta h} & \text{for } d \leqslant z \leqslant d+h \\ \cos\dfrac{\beta z}{a} + a\tanh\beta t\sin\dfrac{\beta z}{a} & \text{for } 0 \leqslant z \leqslant d \\ \dfrac{\cosh\beta(z+t)}{\cosh\beta t} & \text{for } -t \leqslant z \leqslant 0 \end{cases}$$

and

$$A = \frac{J_x(\beta)\sinh\beta(t-s)}{\beta d\cosh\beta t} \cdot \frac{1}{\dfrac{1}{a^2} + \tanh^2\beta t - \dfrac{t}{d}\operatorname{sech}^2\beta t - \dfrac{h}{d}\operatorname{sech}^2\beta h\dfrac{1+a^2\tanh^2\beta t}{1+a^2\tanh^2\beta h}}. \tag{3}$$

The propagation constant β is one of the solutions which satisfies

$$\tan\frac{\beta d}{a} = \frac{a(\tanh\beta t + \tanh\beta h)}{1 - a^2\tanh\beta t\tanh\beta h} \tag{4}$$

where

$$a^2 = -\frac{1}{\mu} = \frac{\Omega^2 - \Omega_H^2}{\Omega_H(\Omega_H+1) - \Omega^2}. \tag{5}$$

Here $\Omega = f/\gamma 4\pi M_s$, $\Omega_H = H/4\pi M_s$, $f = \omega/2\pi$, and $4\pi M_s$, H, and γ are the saturation magnetization, internal dc magnetic field, and gyromagnetic ratio of 2.8 MHz/Oe, respectively.

The potential for the MSFVW propagating in the negative y direction is expressed by (2) if β is replaced by $-\beta$. Hereafter only the dominant mode wave will be considered since it is more easily excited, and has lower loss per unit length than the higher mode waves. In the present paper, a region which is bounded by planes normal to the y axis at edges of each microstrip of the transducer array is called a section of microstrip, and a region between microstrips of the transducer array is referred to as a section of propagation path. Of course, a region between input and output transducers is also a section of the propagation path.

III. Section of Propagation Path

As a first step in the analysis of an MSFVW transducer as an equivalent circuit network, the impedance equivalent of the MSFVW propagation path will be required. The complex Poynting's vector is defined to be $\boldsymbol{S} = -\phi^* \partial\boldsymbol{b}/\partial t$, where ϕ^* is the complex conjugate of ϕ and the vector $\boldsymbol{b}$ is the magnetic flux density. So we define a voltagelike and a currentlike pair by the time derivative of the y component of the magnetic flux density and the magnetic potential. ϕ is given by (2) and $j\omega b_y$ is given by

$$j\omega b_y(y,z) = \omega\mu_0\beta AI_0 f(z) e^{-j\beta y} \tag{6}$$

where

$$f(z) = \begin{cases} \left(\cos\dfrac{\beta d}{a} + a\tanh\beta t\sin\dfrac{\beta d}{a}\right) \cdot \dfrac{\cosh\beta(z-h-d)}{\cosh\beta h} & \text{for } d \leqslant z \leqslant d+h \\ \mu\left(\cos\dfrac{\beta z}{a} + a\tanh\beta t\sin\dfrac{\beta z}{a}\right) & \text{for } 0 \leqslant z \leqslant d \\ \dfrac{\cosh\beta(z+t)}{\cosh\beta t} & \text{for } -t \leqslant z \leqslant 0. \end{cases}$$

We define voltage and current functions so that they may have no transverse-coordinate dependence.

$$j\omega b_y(y,z) = V(y)\frac{1}{K_1}f(z) \tag{7}$$

$$\phi(y,z) = I(y)\frac{1}{K_2}g(z) \tag{8}$$

where K_1 and K_2 are normalizing constants to be determined. From (2), (6), (7), and (8), the wave impedance of the MSFVSW may be defined by

$$Z = \frac{V(y)}{I(y)} = \frac{\omega\mu_0\beta K_1}{K_2}. \tag{9}$$

To determine K_1 and K_2, we proceed in the following manner. The power carried by the traveling waves is

$$W = -\tfrac{1}{2}j\omega\int\int\phi^* b_y\,dz\,dx$$

$$= -\tfrac{1}{2}\omega\mu_0\beta A^2 I_0^2 w\int f(z)g(z)\,dz \tag{10}$$

where w is the YIG film width. It is reasonable that the transmitted power W is correctly given by $VI^*/2$. Thus, from (2), (6), (7), (8), and (10), we have

$$K_1K_2 = -w\int f(z)g(z)\,dz$$

$$= \frac{wd}{2}\left[1+\frac{1}{a^2}-\frac{1+\dfrac{t}{d}}{\cosh^2\beta t}\right.$$

$$\left.-\frac{\dfrac{h}{d}(1+a^2\tanh^2\beta t)}{\cosh^2\beta h(1+a^2\tanh^2\beta h)}\right]. \tag{11}$$

The product K_1K_2 is given by (11) but either K_1 or K_2 is still arbitrary. When K_2 is chosen to be equal to unity, K_1 is considered to be an effective cross section and the MSFVW voltage is measured just in volts. Therefore we adopt it for convenience.

Consider a section of uniform MSFVW propagation path bounded by the planes $y = y_1$ and $y = y_2$ $(> y_1)$. The general transmission line equations for the path section are

$$V = V_+e^{-j\beta y} + V_-e^{j\beta y} \tag{12}$$

$$I = \frac{1}{Z}\left(V_+e^{-j\beta y} - V_-e^{j\beta y}\right). \tag{13}$$

In (12) and (13), V_+ is the complex amplitude of the wave propagating in the positive direction of the y axis and V_- that of the wave in the negative direction. Let the voltages and currents at two ends be V_1, I_1, V_2, and $-I_2$. Here the minus sign is introduced to ensure that the current corresponding to the incoming wave is positive. Imposition of these conditions on (12) and (13) and some manipulations give

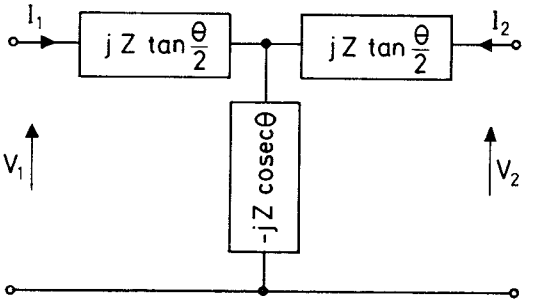

Fig. 3. Equivalent T circuit model for MSFVW propagation path section.

$$V_1 = \frac{Z}{j\sin\theta}(I_1+I_2) + jZ\tan\frac{\theta}{2}I_1 \tag{14}$$

$$V_2 = \frac{Z}{j\sin\theta}(I_1+I_2) + jZ\tan\frac{\theta}{2}I_2 \tag{15}$$

where $\theta = \beta l$ and $l = y_2 - y_1$. From (14) and (15) the equivalent T circuit for the propagation path section can be derived as shown in Fig. 3.

In order to include MSFVW propagation loss, we will find the complex propagation constant. Since YIG films have low intrinsic line widths, use of them allows low propagation losses. Consequently we may obtain the complex propagation constant by a perturbation method. When losses are present, the permeability is given by (5) if H is replaced by $H + j\Delta H/2$. Then a^2 is written approximately as $a^2(1-j2\delta)$. Here δ is given by

$$\delta = \frac{\Delta H}{16\pi M_s}\frac{\Omega^2+\Omega_H^2}{(\Omega^2-\Omega_H^2)\{\Omega_H(\Omega_H+1)-\Omega^2\}}. \tag{16}$$

The propagation constant $\Gamma = j\beta + \alpha$ can be obtained from (4) if a is replaced by $a(1-j\delta)$ and β by $\beta - j\alpha$. Thus the attenuation constant α is given by

$$\alpha = \beta\frac{N}{D}\delta \tag{17}$$

where

$$N = 1+\frac{a^2(\tanh\beta h+\tanh\beta t)(1+a^2\tanh\beta h\tanh\beta t)}{\beta d(1+a^2\tanh^2\beta h)(1+a^2\tanh^2\beta t)}$$

and

$$D = 1-\frac{a^2}{(1+a^2\tanh^2\beta h)(1+a^2\tanh^2\beta t)}\cdot$$

$$\cdot\left\{\frac{h}{d}(1+a^2\tanh^2\beta t)\operatorname{sech}^2\beta h\right.$$

$$\left.+\frac{t}{d}(1+a^2\tanh^2\beta h)\operatorname{sech}^2\beta t\right\}.$$

If there is no ground plane, the loss L is obtained from (17) as follows:

$$L = 76.4\Delta H\frac{\Omega/\Omega_H+\Omega_H/\Omega}{2}\quad \text{dB}/\mu\text{s}. \tag{18}$$

The factor $(\Omega/\Omega_H+\Omega_H/\Omega)/2$ appearing in (18) increases monotonically from unity to $(\Omega_H+1/2)/\sqrt{\Omega_H(\Omega_H+1)}$ when Ω increases from Ω_H to $\sqrt{\Omega_H(\Omega_H+1)}$. If the dc magnetic field is strengthened or the frequency is high, $(\Omega_H+1/2)/\sqrt{\Omega_H(\Omega_H+1)}$ tends to unity. Then (18) agrees with the familiar expression

$$L=76.4\Delta H \qquad \mathrm{dB}/\mu\mathrm{s}. \tag{19}$$

For simplicity the wave impedance Z is still considered real, for α is usually small. Accordingly the propagation losses can be included if θ in Fig. 3 is replaced by $-j\Gamma l$. Now we can treat the MSFVW propagation path as a low-loss transmission line with ports 1 and 2.

IV. Section of Microstrip

In order to analyze the generation and detection of MSFVW, it is necessary to furnish an electric port to the transmission line model developed in the preceding section. Henceforth this electric port is referred to as port 3. To locate port 3, let us consider the current I_3 carried on the microstrip line (Fig. 2) for the generation and detection of MSFVW. The current distribution of I_3 may be considered the x component of $\boldsymbol{n}\times\boldsymbol{h}$ to a first-order approximation. Here $\boldsymbol{n}$ is a unit vector normal to the microstrip. Thus I_3 may be obtained by

$$\begin{aligned} I_3 &= \int_{y_1}^{y_2}(\boldsymbol{n}\times\boldsymbol{h})_x\,dy \\ &= \int_{y_1}^{y_2}\frac{\partial\phi(y,z_0)}{\partial y}\,dy \\ &= \phi(y_2,z_0)-\phi(y_1,z_0)\propto -(I_1+I_2). \end{aligned} \tag{20}$$

Inspection of (20) suggests that port 3 may be connected to the element of $-jZ_s\operatorname{cosec}\theta_s$ in series, as shown in Fig. 4. Here and hereafter the parameters for the microstrip section are distinguished by the subscript s. The lossless transformer is introduced to adjust the coupling between port 3 and the others so that the same amount of power is launched as is done in the YIG film extending indefinitely in the y direction. From (10) and (11) the power radiated in each direction is obtained as $\omega\mu_0\beta K_1A^2I_0^2/2$. Taking bidirectional excitation of the MSFVW into account, the radiation resistance R_m is defined by

$$\tfrac{1}{2}R_mI_0^2=\omega\mu_0\beta K_1A^2I_0^2. \tag{21}$$

Hence

$$R_m=2\omega\mu_0\beta K_1A^2. \tag{22}$$

The input impedance Z_{in} at the transformer terminal pair is readily written as

$$Z_{\mathrm{in}}=\frac{n^2Z}{2}-j\frac{n^2Z_s}{2}\cot\frac{\theta_s}{2}. \tag{23}$$

Putting the first term in (23) equal to (22) yields

$$n^2=\frac{4\omega\mu_0\beta K_1}{Z}A^2. \tag{24}$$

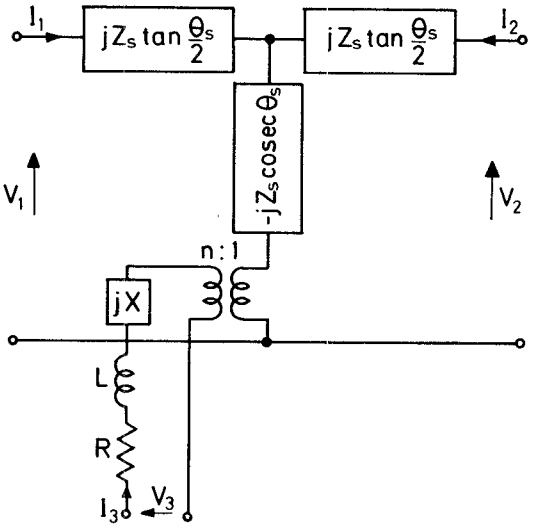

Fig. 4. Equivalent circuit model for a microstrip section.

Substituting (3) and (9) into (24), we obtain

$$n=\frac{2J_x(\beta)\sinh\beta(t-s)}{\beta d\cosh\beta t}\cdot D\frac{1}{\dfrac{1}{a^2}+\tanh^2\beta t-\dfrac{t}{d}\operatorname{sech}^2\beta t-\dfrac{h}{d}\operatorname{sech}^2\beta h\dfrac{1+a^2\tanh^2\beta t}{1+a^2\tanh^2\beta h}}. \tag{25}$$

The series reactance X provides a means of making the equivalent circuit of Fig. 4 satisfy causality. This reactance is given by

$$X=\frac{1}{2}\mathscr{H}(n^2Z)+\frac{1}{2}n^2Z_s\cot\frac{\beta_s l}{2} \tag{26}$$

where $\mathscr{H}$ denotes the Hilbert transform [16], defined by

$$\mathscr{H}(n^2Z)=\frac{1}{\pi}\int_{-\infty}^{\infty}\frac{n^2(x)Z(x)}{x-\omega}\,dx. \tag{27}$$

The evaluation of (27) is carried out by a method shown in Appendix I.

Furthermore, the microstrip line itself is considered to behave like a series circuit of an inductor and a resistor, because a small section of it is terminated in a short circuit. The microstrip lines have been analyzed in many articles. However, to the present authors' knowledge, the microstrip line shown in Fig. 1 has never been studied. Besides, it is difficult to analyze it. So the values of the elements are assumed to be approximated by those of the microstrip line on a dielectric substrate. For a microstrip line of width l on a substrate of thickness u, the formulas per unit length for $l/u\leqq 1$ are given below [17]:

$$L=(\epsilon_0\mu_0)^{1/2}60\ln\left(\frac{8u}{l}+\frac{l}{4u}\right) \qquad \mathrm{H/m} \tag{28}$$

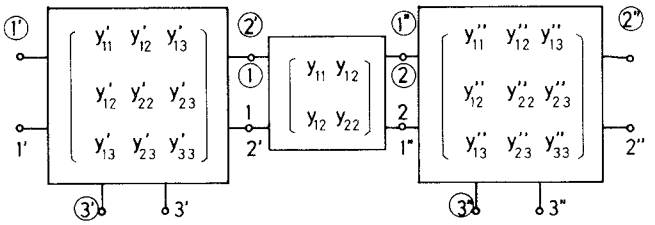

Fig. 5. Cascade connection of MSW ports of three networks.

and

$$R = \frac{R_s}{u} \frac{\left(\frac{8u}{l} - \frac{l}{4u}\right)\left(1 + \frac{u}{l} + \frac{u}{l}r\right)}{\pi\left(\frac{8u}{l} + \frac{l}{4u}\right)} \quad \Omega/\text{m} \qquad (29)$$

where

$$r = \begin{cases} \dfrac{1}{\pi} \ln \dfrac{4\pi l}{\Delta} & \text{for } \dfrac{l}{u} \leqq \dfrac{1}{2\pi} \\ \dfrac{1}{\pi} \ln \dfrac{2u}{\Delta} & \text{for } \dfrac{l}{u} \geqq \dfrac{1}{2\pi} \end{cases}$$

and

$$R_s = (\pi \mu_0 f \rho)^{1/2} \quad \Omega.$$

Here ϵ_0, Δ, and ρ are the permittivity of free space, the thickness of microstrip, and the resistivity of the microstrip conductor, respectively. For the flipped configuration u becomes equal to the difference $t - s$.

V. Multielement Microstrip Transducers

Having formulated the equivalent circuits for both sections of the propagation path and microstrip, the entire microstrip transducer can now be treated as a circuit network. In order to achieve any desired frequency response, the array of microstrips must be weighted by varying the separation between strip centers and the widths of successive strips or reversing the current direction of some groups of strips. No periodicity of the array will be assumed for analysis of such nonuniform arrays.

As can be seen from Fig. 4, a microstrip section is represented by a 3×3 symmetric admittance matrix, of which elements y_{ij} are listed in Appendix II-A. Referring to Fig. 3, a space section between microstrips is also represented by another 2×2 admittance matrix, and its elements y_{ij} are given in Appendix II-B. Cascading these networks as shown in Fig. 5, we obtain a new four-port network which is represented by

$$\begin{pmatrix} I_1' \\ I_2'' \\ I_3' \\ I_3'' \end{pmatrix} = \begin{pmatrix} Y_{11} & Y_{12} & Y_{13} & Y_{14} \\ Y_{12} & Y_{22} & Y_{23} & Y_{24} \\ Y_{13} & Y_{23} & Y_{33} & Y_{34} \\ Y_{14} & Y_{24} & Y_{34} & Y_{44} \end{pmatrix} \begin{pmatrix} V_1' \\ V_2'' \\ V_3' \\ V_3'' \end{pmatrix}. \qquad (30)$$

The values of Y_{ij} are given in Appendix II-C.

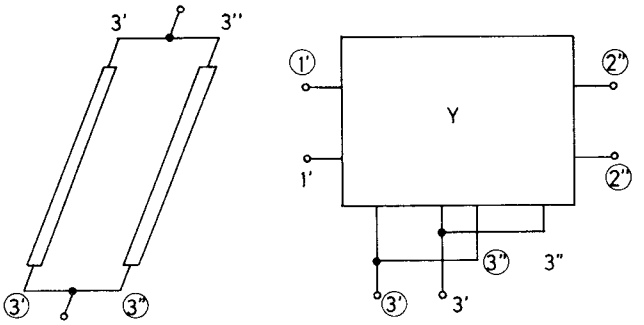

Fig. 6. Parallel connection of two microstrips.

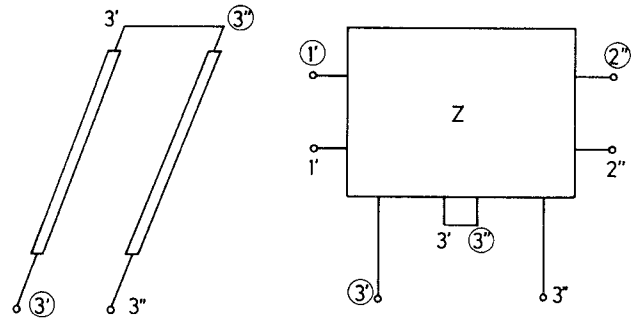

Fig. 7. Series connection of two microstrips.

Connecting the electric ports, the four-port network can be reduced to a three-port one. The resulting three-port network is combined with other three-port and two-port networks. The above procedure will be continued until the entire microstrip array has been connected. The two ports $3'$ and $3''$ of the network of Fig. 5 may be connected in series or in parallel. Let us first consider the parallel connection shown in Fig. 6. From (30) the admittance matrix can be simply written as

$$\begin{pmatrix} Y_{11} & Y_{12} & Y_{13} + Y_{14} \\ Y_{12} & Y_{22} & Y_{23} + Y_{24} \\ Y_{13} + Y_{14} & Y_{23} + Y_{24} & Y_{33} + 2Y_{34} + Y_{44} \end{pmatrix}. \qquad (31)$$

With a series connection of the type shown in Fig. 7, the admittance matrix of (30) is inverted to an impedance matrix. Then the series connection of ports $3'$ and $3''$ reduces the 4×4 impedance matrix to a 3×3 impedance matrix:

$$\begin{bmatrix} Z_{11} & Z_{12} & Z_{13} + Z_{14} \\ Z_{12} & Z_{22} & Z_{23} + Z_{24} \\ Z_{13} + Z_{14} & Z_{23} + Z_{24} & Z_{33} + 2Z_{34} + Z_{44} \end{bmatrix}. \qquad (32)$$

Here it is noted that the turn ratio n given by (25) depends on the Fourier transform of the current distribution. Accordingly it is necessary to reverse the polarity of the transformer of Fig. 4 corresponding to the current direction. So the admittance matrix for an appropriate microstrip section must be computed by substituting $-n$ for n. The inversion of (32) yields an admittance matrix. For such transducers as multibar π, each group of successive microstrips is first represented by a 3×3 admittance ma-

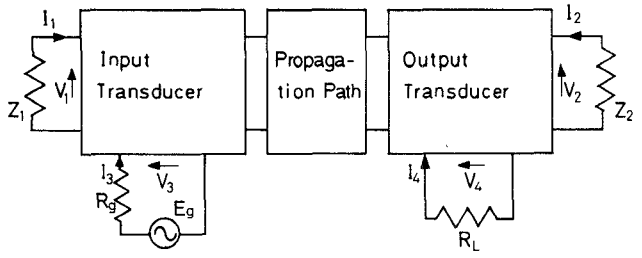

Fig. 8. Complete representation of MSW delay line.

trix, noticing the current direction. Thus the entire transducer can be represented by a 3×3 admittance matrix.

An MSFVW delay line consisting of an input transducer and an output transducer separated by a finite distance can be treated as the three separate admittance matrices developed above. The cascade combination of the networks for the input and output transducers and propagation path forms a new four-port network with ports 1, 2, 3, and 4, as shown in Fig. 8. An admittance matrix for this four-port network can be written in a manner similar to (30). The termination of ports 1 and 2 with the wave impedances Z_1 and Z_2 leads to the following matrix equation:

$$\begin{pmatrix} I_3 \\ I_4 \end{pmatrix} = \begin{pmatrix} \eta_{11} & \eta_{12} \\ \eta_{12} & \eta_{22} \end{pmatrix} \begin{pmatrix} V_3 \\ V_4 \end{pmatrix}. \tag{33}$$

The three admittance parameters η_{ij} are listed in Appendix II-D. Generator E_g, which has an internal resistance R_g, is connected at port 3. The load resistance at port 4 is R_L. Then the insertion loss is given in decibels by

$$IL = -20 \cdot \log_{10} \left| \frac{2\sqrt{R_g R_L}\,\eta_{12}}{1+\eta_{11}R_g+\eta_{22}R_L+R_gR_L(\eta_{11}\eta_{22}-\eta_{12}^2)} \right|. \tag{34}$$

VI. Experiment

To test the equivalent circuit model, some MSFVW transducer pairs were photolithographically fabricated in about 2 μm thick aluminum vacuum-deposited on 300 μm thick sapphire substrates. Individual microstrips in the array were 25 μm wide. The measured values for the separation between bar centers were 158 μm for the input loop transducer; 155 μm for the output loop transducer; 308 μm for the 2 bar parallel transducer pair; 308, 150, and 308 μm for the input 4 bar π transducer; and 303, 158, and 300 μm for the output 4 bar π transducer. The separation between the centers of the input and output transducer arrays was 10 mm. The epitaxial YIG film was 18.5 μm thick grown on a 400 μm thick GGG substrate and cut 5 mm wide. The FMR line width of the YIG film was 0.78 Oe. The saturation magnetization of the YIG film was found to be 1660 G by measuring the MSSW lower limit f_1 and the MSBVW upper frequency limit f_2 and using the relation $f_1 = f_2 = \gamma\sqrt{H(H+4\pi M_s)}$. In order to reduce reflections from the ends of the sample, the sample was cut in a trapezoidal shape and thin aluminum films were deposited on the ends [9].

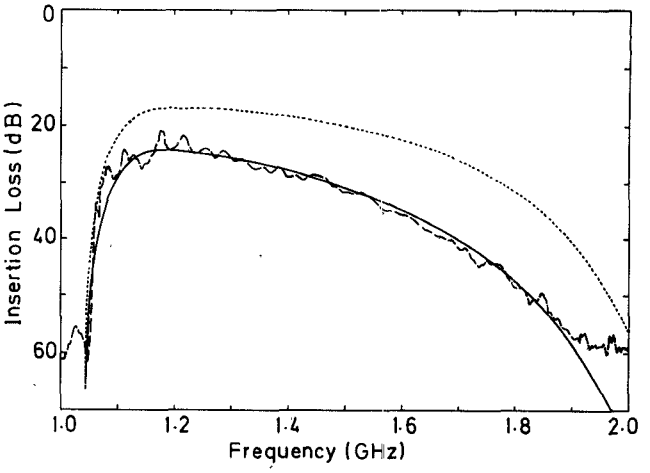

Fig. 9. Insertion loss of a single bar MSFVW transducer pair delay line.

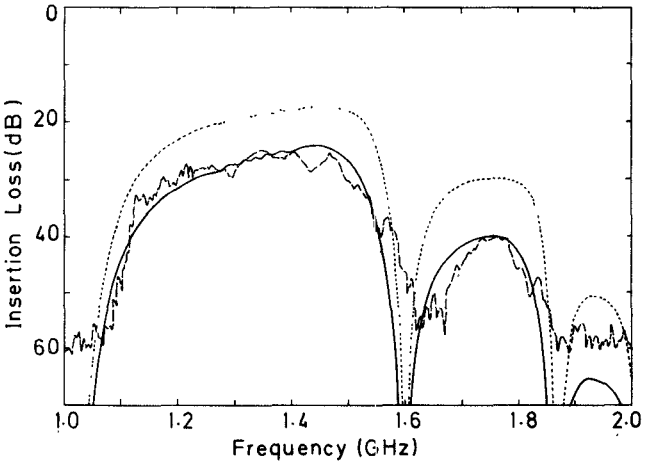

Fig. 10. Insertion loss of a loop transducer pair delay line.

In the computation we adopt a more realistic current distribution [16], $j_x(y) = 1/\pi\sqrt{(l/2)^2 - y^2}$, than a uniform current distribution. Consequently the Fourier transform, $J_0(\beta l/2)$, is substituted for $J_x(\beta)$ in (25). Here J_0 is the Bessel function of order zero.

The insertion losses of the MSFVW delay lines were measured from 1.0 to 2.0 GHz for the single bar, loop, 2 bar parallel, and 4 bar π transducers. The results of these measurements are denoted by the dashed curves in Figs. 9 to 12. The dotted curves are the calculated values of insertion losses as defined by (34). The external magnetic field was measured to be 2080 Oe within ± 100 Oe. The following values are used as internal fields for computation: 370 Oe for the single bar transducer, 360 Oe for the loop transducer, 395 Oe for the 2 bar parallel transducer, and 378 Oe for the 4 bar π transducer. In comparison with the experiments, there are numerous discrepancies in the levels. In the experiment, the transducers were fed through 50 Ω microstrip lines which were 17 mm long and were connected to RF coaxial receptacle center pins by bonding pads. The discrepancies may be due to the shunt capacitances between the bonding pads and the ground conductors and, in part, to the RF coaxial connector to microstrip line transition [18]. Moreover, since the YIG film was

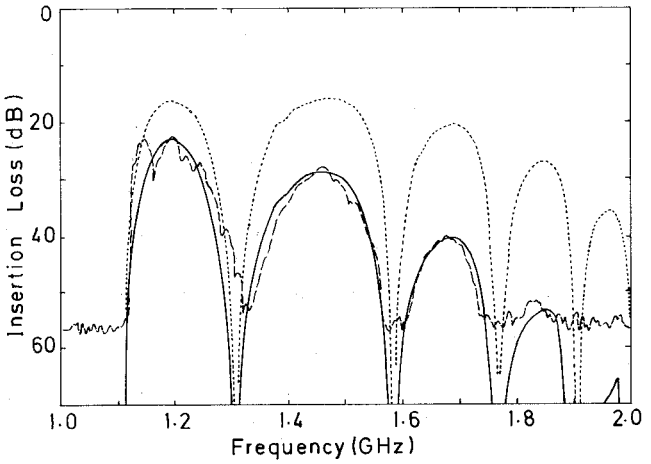

Fig. 11. Insertion loss of a 2 bar parallel strip transducer pair delay line.

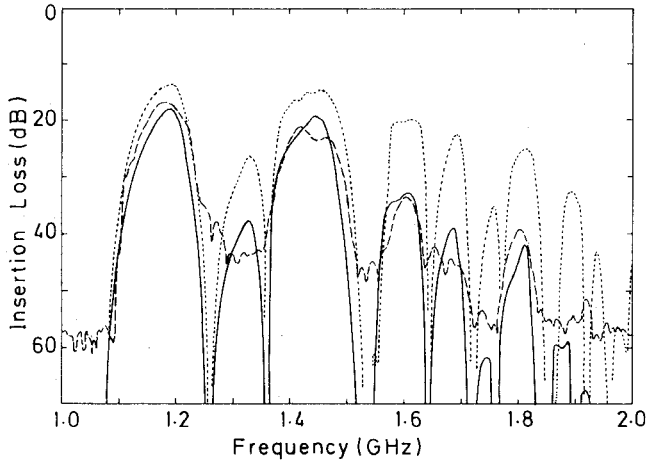

Fig. 12. Insertion loss of a 4 bar π transducer pair delay line.

brought into contact with two microstrip transducers deposited on the sapphire substrate, the YIG film might be considered not to be in intimate contact with the transducers. The calculated values of insertion losses which include these effects are also shown in the figures, by the solid curves. The shunt capacitance and the spacing between the YIG film and transducers were adjusted so that the insertion losses of the experiment and theory might coincide because of the lack of a means to measure them. The assumed shunt capacitances are 3.5 pF for the single bar and loop transducers, 4 pF for the 2 bar parallel transducer, and 3 pF for the 4 bar π transducer. The spacings of the YIG film and transducers were set at 4 μm for the single bar and loop transducers and at 12 μm for the 2 bar parallel and 4 bar π transducers. An excellent agreement between theory and experiment is seen.

VII. Conclusions

The three-port model developed for generation and detection of MSFVW has been demonstrated to be in excellent agreement with experiments. The model can be applied directly to nonuniform arrays of microstrips weighted by varying the separation between strip centers and the

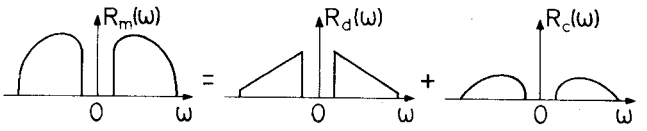

Fig. 13. Decomposition of radiation resistance with jumps into a sum of continuous and discontinuous parts.

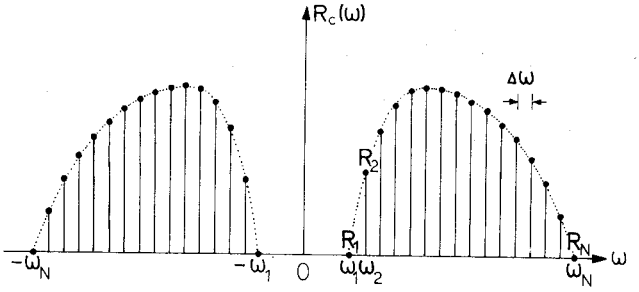

Fig. 14. Discretization for numerical Hilbert transform.

widths of successive strips or reversing the current direction of some groups of strips. The problem still remains for large arrays, wherein the transition region from a microstrip line feed to a transducer microstrip array may occupy a considerable area and have a nonnegligible high capacitance to ground. So we must include this shunt capacitance. Furthermore the electromagnetic coupling between microstrips may need to be considered as mutual inductances or capacitances.

Appendix I
Evaluation of Radiation Reactance

In general, the radiation resistance of MSW R_m may have a jump discontinuity at the lower or upper frequency limit. So R_m will be divided into two parts as shown in Fig. 13, i.e.,

$$R_d(\omega) = \begin{cases} R_l \dfrac{\omega_u - |\omega|}{\omega_u - \omega_l} + R_u \dfrac{|\omega| - \omega_l}{\omega_u - \omega_l} & \text{for } \omega_l \leqslant |\omega| \leqslant \omega_u \\ 0 & \text{for } |\omega| < \omega_l \text{ or } |\omega| > \omega_u \end{cases}$$

and

$$R_c(\omega) = R_m(\omega) - R_d(\omega)$$

where R_l is the value of jump at the lower frequency limit ω_l and R_u is that at the upper frequency limit ω_u.

The discontinuous part of R_m, that is, R_d, can be transformed analytically into

$$\mathcal{H}(R_d) = \frac{1}{\pi}\frac{R_u - R_l}{\omega_u - \omega_l}\omega \ln\left|\frac{(\omega+\omega_u)(\omega-\omega_u)}{(\omega+\omega_l)(\omega-\omega_l)}\right| + \frac{1}{\pi}\frac{R_l\omega_u - R_u\omega_l}{\omega_u - \omega_l}\ln\left|\frac{(\omega+\omega_l)(\omega-\omega_u)}{(\omega+\omega_u)(\omega-\omega_l)}\right|. \quad \text{(A1)}$$

The continuous part R_c will be transformed in the following way. First, R_c is sampled (Fig. 14) and inter-

polated by using sinc functions. Then

$$R_{ci} = \sum_{n=-\infty}^{\infty} R_c(n\Delta\omega)\,\mathrm{sinc}\,\frac{\omega - n\Delta\omega}{\Delta\omega} \tag{A2}$$

where $\Delta\omega$ is a sampling interval. Second, $R_{ci}(\omega)$ is transformed into

$$\mathscr{H}[R_{ci}(\omega)] = X_{ci}(\omega) = -\sum_{n=-\infty}^{\infty} R_c(n\Delta\omega) \cdot \frac{\sin^2[\pi(\omega - n\Delta\omega)/2\Delta\omega]}{\pi(\omega - n\Delta\omega)/2\Delta\omega}. \tag{A3}$$

As a matter of fact the summation is taken for finite values of n since $R_c(\omega)$ vanishes outside the finite frequency band of MSW. Here we put $K = [\omega_l/\Delta\omega]$, where $[x]$ denotes the maximum integer not exceeding x, $N = [\omega_u/\Delta\omega] - K$, $\omega_m = (K+m)\Delta\omega$, and $R_c(\omega_m) = R_m$. Here we replaced K with $K-1$ if $\omega_l = K\Delta\omega$. Finally, for a sampling point within the MSW spectrum band, (A3) becomes

$$X_{ci}(\omega_m) = \frac{4(m+K)}{\pi} \sum_{n=1}^{N}{}' \frac{R_n}{(n+m+2K)(n-m)} \tag{A4}$$

where the prime indicates that the summation is taken over n such that the sum $n+m$ may be an odd number. It can be shown [19] that the maximum error is given by

$$|X_c(\omega) - X_{ci}(\omega)| \leqq \frac{1}{\pi}\int_{|\xi| > \pi/\Delta\omega} |\mathscr{F}[R_c(\omega);\xi]|\,d\xi \tag{A5}$$

where $X_c(\omega)$ is the correct Hilbert transform of $R_c(\omega)$ and $\mathscr{F}[R_c(\omega);\xi]$ is the Fourier transform of $R_c(\omega)$. Since $R_c(\omega)$ behaves as $(\omega-\omega_l)^\tau$ $(\tau>0)$ as ω tends to ω_l, $\mathscr{F}[R_c(\omega);\xi]$ behaves as $\xi^{-(1+\tau)}$ for large ξ [20]. Hence the integral of (A5) exists and $X_{ci}(\omega)$ converges to $X_c(\omega)$ as $\Delta\omega$ tends to zero. Thus the radiation reactance can be computed by taking the sum (A1) and (A4).

Appendix II

A. Admittance Parameters of a Microstrip Section

$$y_{11} = y_{22} = \frac{-j}{Z_s}\,\frac{jn^2 Z_s\cos\theta_s - (R + j\omega L + jX)\sin\theta_s}{jn^2 Z_s\sin\theta_s - 2(R+j\omega L+jX)(1-\cos\theta_s)}$$

$$y_{12} = y_{21} = \frac{j}{Z_s}\,\frac{jn^2 Z_s - (R + j\omega L + jX)\sin\theta_s}{jn^2 Z_s\sin\theta_s - 2(R+j\omega L+jX)(1-\cos\theta_s)}$$

$$y_{13} = y_{31} = y_{23} = y_{32} = \frac{n(1-\cos\theta_s)}{jn^2 Z_s\sin\theta_s - 2(R+j\omega L+jX)(1-\cos\theta_s)}$$

$$y_{33} = \frac{-2(1-\cos\theta_s)}{jn^2 Z_s\sin\theta_s - 2(R+j\omega L+jX)(1-\cos\theta_s)} \tag{A6}$$

B. Admittance Parameters of a Propagation Path Section

$$y_{11} = y_{22} = \frac{-j}{Z}\cot\theta$$

$$y_{12} = y_{21} = \frac{j}{Z\sin\theta} \tag{A7}$$

C. Admittance Parameters of (30)

$$Y_{11} = y'_{11} - \frac{(y_{22}+y''_{11})y'^2_{12}}{(y_{11}+y'_{22})(y_{22}+y''_{11}) - y^2_{12}}$$

$$Y_{12} = \frac{y'_{12}y_{12}y''_{12}}{(y_{11}+y'_{22})(y_{22}+y''_{11}) - y^2_{12}}$$

$$Y_{13} = y'_{13} - \frac{(y_{22}+y''_{11})y'_{23}y'_{12}}{(y_{11}+y'_{22})(y_{22}+y''_{11}) - y^2_{12}}$$

$$Y_{14} = \frac{y'_{12}y_{12}y''_{13}}{(y_{11}+y'_{22})(y_{22}+y''_{11}) - y^2_{12}}$$

$$Y_{22} = y''_{22} - \frac{(y_{11}+y'_{22})y''^2_{12}}{(y_{11}+y'_{22})(y_{22}+y''_{11}) - y^2_{12}}$$

$$Y_{23} = \frac{y'_{23}y_{12}y''_{12}}{(y_{11}+y'_{22})(y_{22}+y''_{11}) - y^2_{12}}$$

$$Y_{24} = y''_{23} - \frac{(y_{11}+y'_{22})y''_{13}y''_{12}}{(y_{11}+y'_{22})(y_{22}+y''_{11}) - y^2_{12}}$$

$$Y_{33} = y'_{33} - \frac{(y_{22}+y''_{11})y'^2_{23}}{(y_{11}+y'_{22})(y_{22}+y''_{11}) - y^2_{12}}$$

$$Y_{34} = \frac{y'_{23}y_{12}y''_{13}}{(y_{11}+y'_{22})(y_{22}+y''_{11}) - y^2_{12}}$$

$$Y_{44} = y''_{33} - \frac{(y_{11}+y'_{22})y''^2_{13}}{(y_{11}+y'_{22})(y_{22}+y''_{11}) - y^2_{12}} \tag{A8}$$

D. Admittance Parameters of (33)

$$\eta_{11} = Y_{33} - \{(Y_{22}+1/Z_2)Y_{13} - Y_{12}Y_{23}\}Y_{13}/\Delta - \{(Y_{11}+1/Z_1)Y_{23} - Y_{12}Y_{13}\}Y_{23}/\Delta$$

$$\eta_{12} = Y_{34} - \{(Y_{22}+1/Z_2)Y_{14} - Y_{12}Y_{24}\}Y_{13}/\Delta - \{(Y_{11}+1/Z_1)Y_{24} - Y_{12}Y_{14}\}Y_{23}/\Delta$$

$$\eta_{22} = Y_{44} - \{(Y_{22}+1/Z_2)Y_{14} - Y_{12}Y_{24}\}Y_{14}/\Delta - \{(Y_{11}+1/Z_1)Y_{24} - Y_{12}Y_{14}\}Y_{24}/\Delta$$

$$\Delta = (Y_{11}+1/Z_1)(Y_{22}+1/Z_2) - Y^2_{12} \tag{A9}$$

Acknowledgment

The authors wish to thank Dr. S. Takeda of the Magnetic & Electronic Materials Research Laboratory, Hitachi Metals, Ltd. for supplying the YIG samples.

References

[1] J M Owens, C. V Smith, Jr., S. N. Lee, and J. H Collins, "Magnetostatic wave propagation through periodic metallic gratings," *IEEE Trans. Magn.*, vol. MAG-14, pp. 820–825, Sept. 1978.

[2] A. K. Ganguly and D. C. Webb, "Microstrip excitation of magnetostatic surface waves: Theory and experiment," *IEEE Trans. Microwave Theory Tech.*, vol. MTT-23, pp. 998–1006, Dec. 1975.
[3] J. D. Adam and S. N. Bajpai, "Magnetostatic forward volume wave propagation in YIG strips," *IEEE Trans. Magn.*, vol. MAG-18, pp. 1598–1600, Nov. 1982.
[4] J. P. Parekh and H. S. Tuan, "Excitation of magnetostatic backward volume waves," *IEEE Trans. Magn.*, vol. MAG-16, pp. 1165–1167, Sept. 1980.
[5] H. J. Wu, C. V. Smith, Jr., J. H. Collins, and J. M. Owens, "Bandpass filtering with multibar magnetostatic-surface-wave microstrip transducers," *Electron. Lett.*, vol. 13, pp. 610–611, Sept. 1977.
[6] J. P. Parekh and H. S. Tuan, "Meander line excitation of magnetostatic surface waves," *Proc. IEEE*, vol. 67, pp. 182–183, Jan. 1979.
[7] J. C. Sethares and I. J. Weinberg, "Apodization of variable coupling MSSW transducers," *J. Appl. Phys.*, vol. 50, pp. 2458–2460, Mar. 1979.
[8] J. C. Sethares, "Magnetostatic surface wave transducers," *IEEE Trans. Microwave Theory Tech.*, vol. MTT-27, pp. 902–909, Nov. 1979.
[9] H. J. Wu, C. V. Smith, Jr., and J. M. Owens, "Bandpass filtering and input impedance characterization for driven multielement transducer pair-delay line magnetostatic wave devices," *J. Appl. Phys.*, vol. 50, pp. 2455–2457, Mar. 1979.
[10] J. P. Parekh, "Theory for magnetostatic forward volume wave excitation," *J. Appl. Phys.*, vol. 50, pp. 2452–2454, Mar. 1979.
[11] I. J. Weinberg, "Insertion loss for magnetostatic volume waves,"*IEEE Trans. Magn.*, vol. MAG-18, pp. 1607–1609, Nov. 1982.
[12] I. J. Weinberg and J. C. Sethares, "Magnetostatic forward volume wave propagation—Finite width," *IEEE Trans. Microwave Theory Tech.*, vol. MTT-32, pp. 463–464, Apr. 1984.
[13] S. N. Bajpai, "Excitation of magnetostatic surface waves: Effect of finite sample width," *J. Appl. Phys.*, vol. 58, pp. 910–913, July 1985.
[14] P. R. Emtage, "Interaction of magnetostatic waves with a current," *J. Appl. Phys.*, vol. 49, pp. 4475–4484, Aug. 1978.
[15] J. M. Owens, R. L. Carter, C. V. Smith, Jr., and G. Hasnian, "A 3-port model for magnetostatic wave transducers," in *Proc. 1980 IEEE Ultrason. Symp.*, 1980, pp. 538–542.
[16] A. K. Ganguly, D. C. Webb, and C. Banks, "Complex radiation impedance of microstrip-excited magnetostatic-surface waves," *IEEE Trans. Microwave Theory Tech.*, vol. MTT-26, pp. 444–447, June 1978.
[17] M. V. Schneider, "Microstrip lines for microwave integrated circuits," *Bell Syst. Tech. J.*, vol. 48, pp. 1421–1444, May/June 1969.
[18] M. R. Daniel, J. D. Adam, and T. W. O'Keeffe, "A linearly dispersive magnetostatic delay line at *X*-band," *IEEE Trans. Magn.*, vol. MAG-15, pp. 1735–1737, Nov. 1979.
[19] K. Yashiro and S. Ohkawa, "Radiation impedance of magnetostatic forward volume wave transducers," in *1987 National Conv. Rec. IEICE Japan*, Mar. 1987, p. 3–217.
[20] T. T. Taylor, "Design of line-source antennas for narrow beamwidth and low side lobes," *IRE Trans. Antennas Propagat.*, vol. AP-3, pp. 16–28, Jan. 1955.

Ken'ichiro Yashiro (M'83) was born in Osaka, Japan, on May 5, 1950. He received the B.S. and M.S. degrees in electronic engineering from Chiba University, Chiba, Japan, in 1974 and 1976, respectively, and the Ph.D. degree from the Tokyo Institute of Technology, Tokyo, Japan, in 1979.

He joined the Department of Electronic Engineering, Chiba University, as a Research Associate in 1979 and was promoted to Associate Professor in 1987. He has been engaged in research on acoustic wave devices, magnetostatic wave devices, and electromagnetic wave scattering problems.

Dr. Yashiro is a member of the Institute of Electronics, Information and Communication Engineers of Japan.

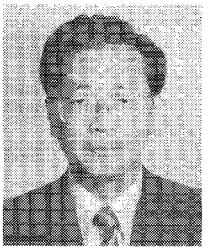

Sumio Ohkawa (M'82–SM'84) was born in Hokkaido, Japan, on July 16, 1935. He received the B.Eng. degree in electrical engineering from Chiba University, Chiba, Japan, in 1961, and the D.eng. degree from the Tokyo Institute of Technology, Tokyo, Japan, in 1974.

He joined the Department of Electrical Engineering of Chiba University as a Research Associate after graduating. In 1970 he transferred to the Department of Electronic Engineering as an Associate Professor, and in 1978 was promoted to full Professor. From October 1979 to July 1980, he studied at the Microwave Research Institute, Polytechnic Institute of New York, as a Visiting Professor. His research has chiefly been concerned with measurements of materials in the microwave range, and now he is also interested in the applications of magnetostatic waves to microwave integrated circuits and electromagnetic wave scattering problems.

Dr. Ohkawa is a member of the Institute of Electronics, Information and Communication Engineers of Japan and a member of the council of Chiba University.